Int. J. Heat Mass Transfer. Vol. 27, No. 6, pp. 829–841, 1984
Printed in Great Britain

0017 9310/84 $3.00 + 0.00
Pergamon Press Ltd.

EFFECT OF A LARGE TEMPERATURE DIFFERENCE AND PYROLYSIS ON THE HEAT TRANSFER BETWEEN A CYLINDER AND TRANSVERSE GAS FLOWS OF NITROGEN AND PROPANE

TOKURO MIZUSHINA, FUMIMARU OGINO, TOSHITATSU MATSUMOTO, HIROSHI UEDA and KAZUYOSHI BABA
Department of Chemical Engineering, Kyoto University, Kyoto, Japan

(*Received* 19 *April* 1983 *and in revised form* 15 *June* 1983)

Abstract—Experimental and analytical investigations have been undertaken for the front boundary-layer region around a heated cylinder normal to cold gas flows. In the flows of propane gas, the usual Nusselt numbers increase significantly with increasing wall temperature in contrast with those of very small variations in the flows of nitrogen. This is caused by the difference of temperature dependencies of fluid properties between both gases and by the pyrolysis of propane at elevated wall temperatures, i.e. at large Damköhler moduli. The results are well represented by the boundary-layer analysis using simple models for reactions and gas compositions. It is also shown that both data for nitrogen and propane at small Damköhler moduli are well correlated regardless of temperature conditions by making use of the Nusselt modulus defined by an enthalpy difference. The experiments, using the heated cylinder 5 mm in diameter and the flows at room temperature and atmospheric pressure, covered the Reynolds numbers from 10^2 to 10^4 and the temperature ratios T_w/T_e from 1.743 to 4.577.

NOMENCLATURE

A	frequency factor in Arrhenius equation, equation (21)
$\hat{C}_p, \hat{C}_{pi}$	specific heat of gas mixture at constant pressure, of component i
D_{ij}	multicomponent diffusivity of the pair i–j, equation (6)
D_{AB}	binary diffusivity for system A–B, equation (22)
E	activation energy of reaction, equation (21)
$\hat{H}, \hat{H}_i$	enthalpy of gas mixture, of component i, per unit mass
$\Delta\hat{H}$	heat of reaction of equation (20) or A → B, per unit mass of A, $\hat{H}_A - \hat{H}_B$
j	mass flux relative to mass averaged velocity
K_{AB}	constant appearing in equation (24), dimensionless
M, M_i	molecular weight of gas mixture, of component i
Nu	Nusselt number, $2Rq_w/(T_w - T_e)\lambda_e$
P	pressure
Pr	Prandtl number, $\hat{C}_p\mu/\lambda$
q	heat flux caused by conduction
R	radius of cylinder
$\hat{R}, \tilde{R}$	gas constants
R_i	molar rate of production of component i
Sc	Schmidt number in binary system A–B, $\mu/\rho D_{AB}$
U	v_{xe}/v_a
U'	$d(v_{xe}/v_a)/d(x/R)$
v	mass averaged velocity
X	x/R
x	distance along cylinder surface from front stagnation point
y	normal distance from cylinder surface
$\hat{y}$	$\int_0^y (\mu_e/\mu)\, dy$.

Greek symbols

α	exponent in equation (31)
β	exponent in equation (34)
γ_k	reaction rate of reaction k given by equation (20), mole per unit volume per second
δ	boundary layer thickness
$\hat{\delta}$	$\int_0^\delta (\mu_e/\mu)\, dy$
$\hat{\eta}$	$\hat{y}/\hat{\delta}$
θ	angle between y-coordinate at front stagnation point and at x
λ	thermal conductivity of gas mixture
μ, μ_i	viscosity of gas mixture, of component i
ρ, ρ_i	density of gas mixture, of component i
σ	Stefan–Boltzmann constant
τ	shear stress
ϕ_{AB}, ϕ_{BA}	coefficients in the formula of Bromley and Wilke [21], dimensionless
Ω	$\rho_e v_a \hat{\delta}^2/\mu_e R$
ω_i	mass fraction of component i in gas mixture, ρ_i/ρ.

Subscripts

A	component A (propane)
a	approaching condition
B	component B (mixture of pyrolysis products)
Di	concentration of component i
H	enthalpy
M	momentum
e	outer edge of boundary layer
i	component i

x	x-direction
y	y-direction
w	wall.

1. INTRODUCTION

HEAT transfer between a circular cylinder and a transverse stream is one of the basic subjects in heat transfer engineering. Experiments have been made in subsonic flows by Schmidt and Wenner [1] and Eckert and co-workers [2, 3]. The theoretical analysis based on the boundary-layer approximation by Frössling [4] and Dieneman [5] agrees well with those experimental results.

However, some points remain to be clarified in the case of a large temperature difference between the wall and ambient flows of gases, especially thermally unstable gases such as light paraffins at elevated temperatures. An interaction between momentum and heat transfers caused by changes of fluid properties due to changes of temperature may result in heat transfer coefficients different from those obtained at a small temperature difference. More important are the effects of pyrolysis in the thermal boundary layer at an elevated temperature.

Concerning the effect of a large temperature difference, a correlation of heat transfer coefficients expressed by fluid properties at film temperature has been conventionally used, since Churchill and co-workers [6, 7] proposed such a correlation in the experiments involving flows in air and nitrogen. However, no investigation has been reported for heat transfer involving flows of organic gases in which the temperature dependencies of the thermal conductivities and specific heats differ from those of air and nitrogen.

Pyrolysis can be regarded as a homogeneous reaction. The treatment of heat transfer with a homogeneous reaction is simplified when the reaction rate is very low or very high. Since the low reaction rate has little effect on the heat transfer, most studies [8, 9] have dealt with the latter case by means of the reaction system $N_2O_4 \rightleftarrows 2NO_2$ in the range 30–150°C. This reaction system is a rapid, reversible and homogeneous reaction with a large enthalpy change and the heat transfer coefficients have been conventionally correlated by using effective thermal conductivity and heat capacity, because the gas composition is a function of temperature.

A few investigators dealt with cases of a finite reaction rate which is a function of both temperature and composition. Brian and Reid [10], and Brian [11] analyzed the effects of reaction on the heat transfer coefficients by using the concept of constant film thickness under the assumption of a small temperature difference. Tambour [12] solved the boundary-layer equations at the stagnation point for the case of combustion of a pre-mixed fuel. The investigations dealing with the pyrolysis system have been made by several investigators; endothermic air dissociations in a high speed boundary-layer flow [13, 14], nitrogen oxide decomposition in a rotating concentric cylinder [15], natural convection around wires [16], and ozone decompositions in a turbulent pipe flow [17]. Nevertheless, it can be said that the heat transfer involving a chemical reaction has not been investigated thoroughly in producing a general theory or applications.

This paper presents the results of an experimental and analytical investigation on heat transfers between a cylinder at 1373 K and a transverse stream of propane at room temperature and atmospheric pressure.

2. EXPERIMENTS

2.1. *Apparatus and procedure*

The schematic diagram of the equipment and the flow system is shown in Fig. 1. Test gases at atmospheric pressure and room temperature were circulated by a blower through an orifice meter, a contraction nozzle, and a rectangular duct. The cross-section of the rectangular duct was 20 mm high and 100 mm wide. To maintain a constant gas composition, fresh gas was supplied at the rate of 3.3×10^{-5} m^3 s^{-1} from a gas container through a rotameter into the main stream while the same amount of gas was exhausted from the main stream through a pressure regulating device and subjected to combustion. A test cylinder was set across the flow at the exit of the contraction nozzle where the velocity and temperature profiles of the flow were flat and the turbulent level low.

As shown in the lower part of Fig. 1, the test cylinder was composed of a stainless steel tube 5 mm in diameter with a wall thickness of 0.3 mm and a porcelain tube with a 2 mm O.D., a net of quartz fiber being packed between them. A chromel–alumel thermocouple with a sheath diameter of 0.5 mm was inserted in the inner tube with its tip portion, 3 mm long, brought into tight contact with the inner wall of the outer stainless steel tube. The angle made by the tip with the horizontal direction of the approaching flow was 55°. Both ends of the stainless steel tube were welded to brass supports which were 70 mm apart. To these supports an alternating electric current was applied and heat was generated by ohmic resistance of the stainless steel tube.

The consumption of electric power per unit area was determined by measuring the electric current and by using the calibrated resistance of the stainless steel tube. The amount of heat transferred by radiation and longitudinal conduction was measured by reducing the pressure in the duct to below 100 N m^{-2} in order to remove the natural convection effect. By subtracting this heat loss by radiation and longitudinal conduction from the consumed electric power, the convective heat flux was determined. The effect of circumferential conduction on the radial heat flux at the wall of the thermocouple location was estimated by assuming a circumferential distribution of the Nusselt number measured by Krall and Eckert [3]. The readings of the thermocouples in the cylinder and in the flow at the mouth of the contraction nozzle were used as values for

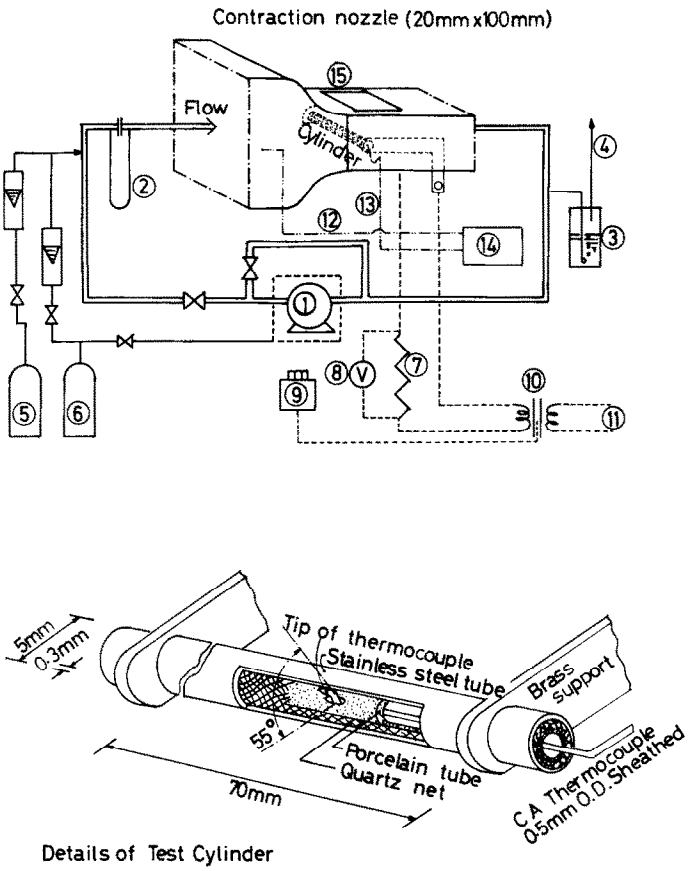

FIG. 1. Schematic diagram of equipment and details of test cylinder: (1) blower; (2) orifice; (3) pressure regulator; (4) to burner; (5) C_3H_8 bomb; (6) N_2 bomb; (7) standard resistance; (8) RMS voltmeter; (9) voltage regulator; (10) power transformer; (11) A.C. 200 V; (12), (13) thermocouples; (14) recorder; (15) window.

the temperature of the cylinder wall and of the outer edge of the boundary layer without any correction, since the temperature change in the wall of the stainless steel tube and that of the flow in the duct is small compared with the large temperature difference between the wall and the flow.

Gases sampled from the exhaust and the inlet tubes were analyzed using FID-gas-chromatography. The Reynolds number based on the cylinder diameter and the fluid properties at approaching conditions ranged from 10^2 to 10^4.

2.2. *Results*

The heat fluxes obtained at a low pressure of 100 N m^{-2} are shown in Fig. 2. The dot-dashed line shows the radiative heat flux with an emissivity of unity. The experimental results are well fitted by a solid line, showing that an apparent emissivity is 0.86, and there is a small contribution of a molecular conductive flux, q_c, to the heat loss. By using this diagram, all experimental data shown in the subsequent figures were corrected. The probable error of the estimated heat loss was calculated to be 5.2% by using the least squares method. In addition, the propane was assumed to be transparent to heat radiation because of no available data on the emissivity.

The experimental results of the heat transfers are shown in Fig. 3. All fluid properties used for the correlations are values at the temperature of

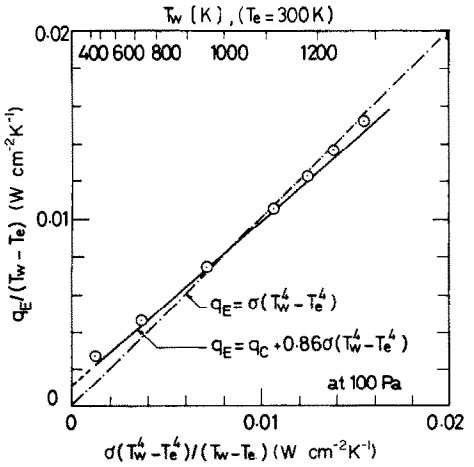

FIG. 2. Experimental results of radiative and conductive heat flux q_E.

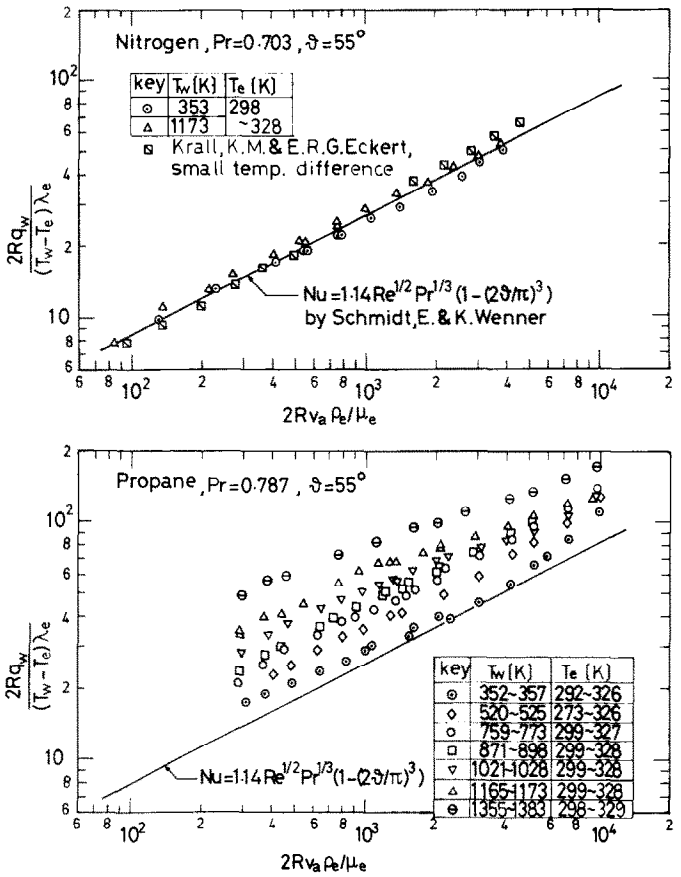

FIG. 3. Experimental results of Nusselt numbers in flows of nitrogen and propane.

approaching flow. The upper figure shows the experimental results for nitrogen flows along with the local values at $\theta = 55°$ obtained by Krall and Eckert [3]. The agreement between the experimental results and the solid line is good.

Contrary to the results for the flow of nitrogen, the values of Nusselt number in flows of propane increase with increasing wall temperature, as seen in the lower part of Fig. 3. The typical gas composition in the duct is shown in Fig. 4. At wall temperatures elevated to more than about 1023 K, yields of methane and ethylene by the cracking of propane are significant, but at temperatures lower than 873 K chemical changes are not noticeable. However, Fig. 3 shows that the change of Nusselt numbers with the wall temperature at the chemically inert temperature, $T_w < 873$ K, is larger than that in the nitrogen flow at much higher wall temperatures.

A more detailed discussion of these results will be given in the subsequent theoretical discussion.

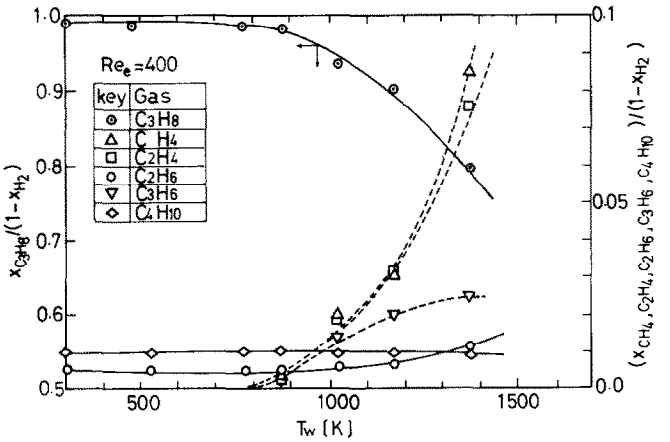

FIG. 4. Typical gas composition of propane flow after test cylinder.

3. DISCUSSIONS

3.1. *Boundary-layer equations and boundary conditions*

The basic boundary-layer equations for conservation of mass, momentum, component i and energy in the flow past a cylinder are given by the following equations

$$\frac{\partial}{\partial x}(\rho v_x)+\frac{\partial}{\partial y}(\rho v_y)=0, \tag{1}$$

$$\frac{\partial}{\partial x}(\rho v_x v_x)+\frac{\partial}{\partial y}(\rho v_y v_x)=\rho_e v_{xe}\frac{\mathrm{d}v_{xe}}{\mathrm{d}x}-\frac{\partial \tau_{xy}}{\partial y}, \tag{2}$$

$$\frac{\partial}{\partial x}(\rho\omega_i v_x)+\frac{\partial}{\partial y}(\rho\omega_i v_y)=-\frac{\partial j_{iy}}{\partial y}+M_i R_i, \tag{3}$$

$$\frac{\partial}{\partial x}\left\{\left(\sum_{i=1}^{n}\omega_i\hat{H}_i\right)\rho v_x\right\}+\frac{\partial}{\partial y}\left\{\left(\sum_{i=1}^{n}\omega_i\hat{H}_i\right)\rho v_y\right\}=-\frac{\partial q_y}{\partial y}-\frac{\partial}{\partial y}\left(\sum_{i=1}^{n}\hat{H}_i j_{iy}\right), \tag{4}$$

where $\omega_i=\rho_i/\rho$ denotes the mass fraction of species i. The coordinate system is depicted in Fig. 5. The second terms on the RHS of equations (3) and (4) are the rate of production of species i by chemical reaction and the energy transfer caused by interdiffusion, respectively. The shear stress, mass flux of component i and heat flux are given by

$$\tau_{xy}=-\mu\frac{\partial v_x}{\partial y}, \tag{5}$$

$$j_{iy}=\rho\sum_{j=1}^{n}\frac{M_i M_j}{M^2}D_{ij}\frac{\partial}{\partial x}\left(\frac{M}{M_j}\omega_j\right), \tag{6}$$

and

$$q_y=-\lambda\frac{\partial T}{\partial y}. \tag{7}$$

Equations (1)–(4) are to be solved with the boundary conditions:

$$\left.\begin{aligned}\text{at } y=0;\quad & v_x=0, \quad v_y=0,\\ & j_{iy}=0,\\ & q_y=q_w, \quad T=T_w,\end{aligned}\right\} \tag{8}$$

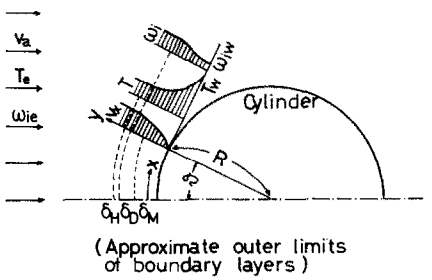

FIG. 5. Coordinate system for two-dimensional flow around a cylinder.

$$\left.\begin{aligned}\text{at } y=\infty;\quad & \tau_{xy}=0, \quad v_x=v_{xe},\\ & j_{iy}=0, \quad \omega_i=\omega_{ie},\\ & q_y=0, \quad T=T_e.\end{aligned}\right\} \tag{9}$$

It is difficult, however, to solve the set of simultaneous differential equations (1)–(4).

We now attempt to get an approximate solution by using an integral method. For this purpose we provide the boundary-layer thickness δ_M for velocity, δ_{Di} for concentration of component i and δ_H for enthalpy. In the present analysis we assume that $\delta_H>\delta_M$ because $Pr<1$. Then, from equations (2)–(4) we obtain the macroscopic balances of the momentum, component i and enthalpy in the boundary layers as

$$\tau_w=\frac{\mathrm{d}}{\mathrm{d}x}\int_0^{\delta_M}\rho v_x(v_x-v_{xe})\,\mathrm{d}y+\frac{\mathrm{d}v_{xe}}{\mathrm{d}x}\int_0^{\delta_M}(\rho v_x-\rho_e v_{xe})\,\mathrm{d}y, \tag{10}$$

$$\int_0^{\delta_{Di}}M_i R_i\,\mathrm{d}y=\frac{\mathrm{d}}{\mathrm{d}x}\int_0^{\delta_{Di}}\rho v_x(\omega_i-\omega_{ie})\,\mathrm{d}y, \tag{11}$$

and

$$q_w=\frac{\mathrm{d}}{\mathrm{d}x}\int_0^{\delta_H}\rho v_x\left(\sum_{i=1}^{n}\omega_i\hat{H}_i-\sum_{i=1}^{n}\omega_{ie}\hat{H}_{ie}\right)\mathrm{d}y. \tag{12}$$

We assume polynomials of the third order for the shear stress, mass flux of component i and enthalpy flux in terms of the dimensionless distance from the wall, i.e.

$$\left.\begin{aligned}&(\tau_{xy}-\tau_w)/\tau_w=\sum_{n=0}^{3}a_n(\hat{\eta}_M)^n,\\ &j_{iy}=\sum_{n=0}^{3}b_n(\hat{\eta}_{Di})^n,\\ \text{and}\quad &\left(q_y-q_w+\sum_{i=1}^{n}\hat{H}_i j_{iy}\right)\Big/q_w=\sum_{n=0}^{3}c_n(\hat{\eta}_H)^n.\end{aligned}\right\} \tag{13}$$

The dimensionless distances from the wall $\hat{\eta}_M$, $\hat{\eta}_H$ and $\hat{\eta}_{Di}$ are given by

$$\hat{\eta}_M=\hat{y}/\hat{\delta}_M,\quad \hat{\eta}_{Di}=\hat{y}/\hat{\delta}_{Di}\quad\text{and}\quad \hat{\eta}_H=\hat{y}/\hat{\delta}_H, \tag{14}$$

where

$$\hat{y}=\int_0^{y}(\mu_e/\mu)\,\mathrm{d}y$$

and

$$\hat{\delta}_{M,Di,H}=\int_0^{\delta_{M,Di,H}}(\mu_e/\mu)\,\mathrm{d}y.$$

The coefficients in the polynomials are determined by the following boundary conditions which are all

satisfied by the exact solutions

$$\left.\frac{\partial \tau_{xy}}{\partial y}\right|_{y=0} = \rho_e v_{xe}\frac{dv_{xe}}{dx},$$

$$\left.\frac{\partial \tau_{xy}}{\partial y}\right|_{y=\delta_M} = \rho_e v_{xe}\frac{dv_{xe}}{dx}\left(1-\frac{\rho_{\delta_M}}{\rho_e}\right),$$

$$\left.\tau_{xy}\right|_{y=0} = 0, \quad \left.\frac{\partial j_{iy}}{\partial y}\right|_{y=0} = M_i R_{iw},$$

$$\left.\frac{\partial j_{iy}}{\partial y}\right|_{y=\delta_{Di}} = M_i R_{ie}, \quad \left.j_{iy}\right|_{y=0} = 0,$$

$$\left.j_{iy}\right|_{y=\delta_{Di}} = 0, \quad \left.\frac{\partial}{\partial y}\left(q_y + \sum_{i=1}^{n}\hat{H}_i j_{iy}\right)\right|_{y=0} = 0,$$

$$\left.\frac{\partial}{\partial y}\left(q_y + \sum_{i=1}^{n}\hat{H}_i j_{iy}\right)\right|_{y=\delta_H} = 0 \quad \text{and} \quad \left.q_y\right|_{y=\delta_H} = 0.$$

Consequently the profiles of shear stress, mass flux of component i and heat flux are

$$\frac{(\tau_{xy}-\tau_w)}{-\tau_w} = (3\hat{\eta}_M^2 - 2\hat{\eta}_M^3) - \left(\frac{\mu_w}{\mu_e}\right)\frac{\rho_e v_{xe}\hat{\delta}_M}{\tau_w}\frac{dv_{xe}}{dx}(\hat{\eta}_M - 2\hat{\eta}_M^2 + 3\hat{\eta}_M^3) + \left(\frac{\mu_{e'}}{\mu_e}\right)\left(1-\frac{\rho_{e'}}{\rho_e}\right)\frac{\rho_e v_{xe}\hat{\delta}_M}{\tau_w}\frac{dv_{xe}}{dx}(\hat{\eta}_M^2 - \hat{\eta}_M^3), \quad (15)$$

$$\frac{j_{iy}}{M_i R_{ie}\hat{\delta}_{Di}} = \left(\frac{\mu_w}{\mu_e}\right)\left(\frac{R_{iw}}{R_{ie}}\right) \times (\hat{\eta}_{Di} - 2\hat{\eta}_{Di}^2 + \hat{\eta}_{Di}^3) - (\hat{\eta}_{Di}^2 - \hat{\eta}_{Di}^3), \quad (16)$$

and

$$\frac{\left(q_y - q_w + \sum_{i=1}^{n}\hat{H}_i j_{iy}\right)}{-q_w} = (3\hat{\eta}_H^2 - 2\hat{\eta}_H^3), \quad (17)$$

where $\mu_{e'}$ and $\rho_{e'}$ denote the values at $y = \delta_M$.

Then, the velocity profile and the wall shear stress are obtained by using equations (5) and (15) and the boundary conditions as

$$\frac{v_x}{v_{xe}} = (2\hat{\eta}_M - 2\hat{\eta}_M^3 + \hat{\eta}_M^4) + \frac{1}{6}\left(\frac{\mu_w}{\mu_e}\right)U'\Omega_M(\hat{\eta}_M - 3\hat{\eta}_M^2 + 3\hat{\eta}_M^3 - \hat{\eta}_M^4) - \frac{1}{6}\left(\frac{\mu_{e'}}{\mu_e}\right)\left(1-\frac{\rho_{e'}}{\rho_e}\right)U'\Omega_M(\hat{\eta}_M - 3\hat{\eta}_M^3 + 2\hat{\eta}_M^4), \quad (18)$$

$$\frac{-\tau_w\hat{\delta}_M}{\mu_e v_{xe}} = 2 + \frac{1}{6}\left(\frac{\mu_w}{\mu_e}\right)U'\Omega_M - \frac{1}{6}\left(\frac{\mu_{e'}}{\mu_e}\right)\left(1-\frac{\rho_{e'}}{\rho_e}\right)U'\Omega_M, \quad (19)$$

where

$$U' = \frac{d(v_{xe}/v_a)}{d(x/R)},$$

and

$$\Omega_M = \frac{\rho_e v_a \hat{\delta}_M^2}{\mu_e R}.$$

To obtain the concentration profile, it is necessary to know D_{ij} in equation (6). The pyrolysis of propane follows a complex process even if chemically stable components are used for modeling the reaction [18]

(First)

$$C_3H_8 \xrightarrow{\gamma_1} 0.34H_2 + 0.59CH_4 + 0.07C_2H_6 + 0.52C_2H_4 + 0.41C_3H_6,$$

(Successive)

$$C_2H_6 \underset{\gamma_3}{\overset{\gamma_2}{\rightleftarrows}} H_2 + C_2H_4, \quad C_2H_4 \xrightarrow{\gamma_4} H_2 + C_2H_2, \quad C_3H_6 + H_2 \xrightarrow{\gamma_5} CH_4 + C_2H_4, \quad \text{etc.} \quad (20)$$

However, only the first reaction is important because successive reactions have smaller rates. The rate of the first reaction is given by [18]

$$\gamma_1 = A\left(\rho\frac{\omega_A}{M_A}\right)^{3/2}\exp\left(-\frac{E}{\tilde{R}T}\right), \quad (21)$$

where $A = 6.9 \times 10^{10}$ mol$^{-3/2}$ m$^{3/2}$ and $E = 2.156 \times 10^5$ J mol^{-1}. Moreover, to simplify the calculation procedure the system is assumed to be a binary system of propane (subscript A) and a mixture of products (subscript B).

Thus, equation (6) becomes

$$j_{iy} = j_{Ay} = -j_{By} = -\rho D_{AB}\frac{\partial \omega_A}{\partial y}, \quad (22)$$

and the diffusivity D_{AB} can be calculated from the equation of Fujita [19]. From equations (16) and (22) one can obtain

$$\left(\frac{\rho_e D_{ABe}}{-M_A R_{Ae}\hat{\delta}_D^2}\right)\left(\frac{Sc_e}{Sc}\right)\frac{\partial \omega_A}{\partial \hat{\eta}_D} = \left(\frac{\mu_w}{\mu_e}\right)\left(\frac{R_{Aw}}{R_{Ae}}\right) \times (\hat{\eta}_D - 2\hat{\eta}_D^2 + \hat{\eta}_D^3) - (\hat{\eta}_D^2 - \hat{\eta}_D^3). \quad (23)$$

Integration of equation (23) under the boundary conditions gives

$$\omega_A = \frac{\omega_{Aw}K_{AB}+1}{K_{AB}}\xi - \frac{1}{K_{AB}}, \quad (24)$$

where

$$\xi = \exp\left\{\frac{(\mu_w/\mu_e)(R_{Aw}/R_{Ae})(6\hat{\eta}_D^2 - 8\hat{\eta}_D^3 + 3\hat{\eta}_D^4) - (4\hat{\eta}_D^3 - 3\hat{\eta}_D^4)}{(\mu_w/\mu_e)(R_{Aw}/R_{Ae}) - 1}\ln\left(\frac{\omega_{Ae}K_{AB}+1}{\omega_{Aw}K_{AB}+1}\right)\right\},$$

and K_{AB} is a constant in an approximation of $Sc/Sc_e \simeq (\omega_A K_{AB}+1)/(\omega_{Ae}K_{AB}+1)$ derived from Wilke's equation [21]. The concentration at the wall, ω_{Aw}, can be calculated from

$$\left(\frac{-M_A R_{Ae} R}{\rho_e v_a}\right)\Omega_D\, Sc_e = \frac{((\omega_{Ae}K_{AB}+1)/K_{AB})\ln((\omega_{Ae}K_{AB}+1)/(\omega_{Aw}K_{AB}+1))}{(1/12)\{(\mu_w/\mu_e)(R_{Aw}/R_{Ae})-1\}} \quad (25)$$

where

$$\Omega_D = \frac{\rho_e v_a \hat{\delta}_D^2}{\mu_e R}.$$

Since the change of the enthalpy $\hat{H} = \sum_{i=1}^{n} \hat{H}_i \omega_i$ is expressed as

$$d\hat{H} = \sum_{i=1}^{n} \left(\hat{H}_i \, d\omega_i + \omega_i \frac{d\hat{H}_i}{dT} dT \right) = \sum_{i=1}^{n} \hat{H}_i \, d\omega_i + \hat{C}_p \, dT, \tag{26}$$

equation (7) is rewritten as

$$q_y = -\lambda \frac{\partial T}{\partial y} = -\frac{\lambda}{\hat{C}_p} \frac{\partial \hat{H}}{\partial y} + \frac{\lambda}{\hat{C}_p} \sum_{i=1}^{n} \left(\hat{H}_i \frac{\partial \omega_i}{\partial y} \right). \tag{27}$$

Also, in the present binary system the enthalpy flux caused by the mass flux is

$$\sum_{i=1}^{n} \hat{H}_i j_{iy} = \hat{H}_A j_{Ay} + \hat{H}_B j_{By} = (\hat{H}_A - \hat{H}_B) j_{Ay} = \Delta\hat{H} j_{Ay}. \tag{28}$$

$\Delta\hat{H} = (\hat{H}_A - \hat{H}_B)$ is the heat of reaction per unit mass of propane, which is a nearly constant value in a temperature range from room temperature to 1500 K.

Thus, by using equations (17), (27) and (28) we get

$$\frac{\hat{H} - \hat{H}_e}{\hat{H}_w - \hat{H}_e} = 1 - \left\{ 1 + \left(\frac{-\Delta\hat{H}}{\hat{H}_w - \hat{H}_e} \right) \times \left(\frac{Pr}{Sc_e} \frac{\omega_{Ae} K_{AB} + 1}{K_{AB}} \ln \left(\frac{\omega_{Ae} K_{AB} + 1}{\omega_{Aw} K_{AB} + 1} \right) - (\omega_{Ae} - \omega_{Aw}) \right) \right\} (2\hat{\eta}_H - 2\hat{\eta}_H^3 + \hat{\eta}_H^4) + \left(\frac{-\Delta\hat{H}}{\hat{H}_w - \hat{H}_e} \right) \times \left\{ \frac{Pr}{Sc_e} \frac{\omega_{Ae} K_{AB} + 1}{K_{AB}} \ln \left(\frac{\omega_A K_{AB} + 1}{\omega_{Aw} K_{AB} + 1} \right) - (\omega_A - \omega_{Aw}) \right\}, \tag{29}$$

$$\frac{Pr \, q_w \hat{\delta}_H}{\mu_e (\hat{H}_w - \hat{H}_e)} = 2 \left\{ 1 + \left(\frac{-\Delta\hat{H}}{\hat{H}_w - \hat{H}_e} \right) \times \left(\frac{Pr}{Sc_e} \frac{\omega_{Ae} K_{AB} + 1}{K_{AB}} \ln \left(\frac{\omega_{Ae} K_{AB} + 1}{\omega_{Aw} K_{AB} + 1} \right) - (\omega_{Ae} - \omega_{Aw}) \right) \right\}. \tag{30}$$

In these calculations, Pr has been regarded as a constant and $\hat{\delta}_H > \hat{\delta}_D$ has been implicitly assumed. The relationship between $\hat{\delta}_H$ and $\hat{\delta}_D$ may change with Pr, Sc_e, $(E/\tilde{R}T_e)$, (T_w/T_e), $(\Delta\hat{H}/(\hat{H}_w - \hat{H}_e))$ and $(M_A R_{Ae} R/\rho_e v_a)$, but the relationship $\hat{\delta}_H > \hat{\delta}_D$ is valid in the present system of $T_e \simeq 300$ K, $T_w \leqslant 1373$ K and $\psi = (M_a A (P/\tilde{R}T_e)^{3/2} R/\rho_e v_a) \leqslant 209.5 \times 10^8$.

To obtain the temperature profile, we use an approximation

$$\left(\frac{\lambda}{\lambda_e} \frac{\mu_e}{\mu} \right) \simeq \left(\frac{T}{T_e} \right)^{\alpha}. \tag{31}$$

Then, by a similar treatment for the enthalpy profile, the temperature profile is obtained as

$$\left(\frac{T}{T_e} \right)^{1+\alpha} = \left(\frac{T_w}{T_e} \right)^{1+\alpha} + \left\{ \left(1 - \left(\frac{T_w}{T_e} \right)^{1+\alpha} \right) + (1+\alpha) \times \left(\frac{-\Delta\hat{H}\mu_e}{\lambda_e T_e} \right) \frac{1}{Sc_e} \frac{\omega_{Ae} K_{AB} + 1}{K_{AB}} \ln \left(\frac{\omega_{Ae} K_{AB} + 1}{\omega_{Aw} K_{AB} + 1} \right) \right\} \times (2\hat{\eta}_H - 2\hat{\eta}_H^3 + \hat{\eta}_H^4) + (1+\alpha) \left(\frac{-\Delta\hat{H}\mu_e}{\lambda_e T_e} \right) \frac{1}{Sc_e} \times \frac{\omega_{Ae} K_{AB} + 1}{K_{AB}} \ln \left(\frac{\omega_A K_{AB} + 1}{\omega_{Aw} K_{AB} + 1} \right), \tag{32}$$

and the wall heat flux as

$$\left(\frac{-q_w \hat{\delta}_H}{\lambda_e T_e} \right) = \frac{2}{1+\alpha} \left\{ \left(1 - \left(\frac{T_w}{T_e} \right)^{1+\alpha} \right) - (1+\alpha) \left(\frac{-\Delta\hat{H}\mu_e}{\lambda_e T_e} \right) \times \frac{1}{Sc_e} \frac{\omega_{Ae} K_{AB} + 1}{K_{AB}} \ln \left(\frac{\omega_{Ae} K_{AB} + 1}{\omega_{Aw} K_{AB} + 1} \right) \right\}. \tag{33}$$

Using equation (32), local changes of density and viscosity with temperature can be calculated.

Substituting the profiles presented above into equations (10)–(12), we get simultaneous differential equations concerning $\Omega_M = (\rho_e v_a \hat{\delta}_M^2/\mu_e R)$, $\Omega_D = (\rho_e v_a \hat{\delta}_D^2/\mu_e R)$, $\Omega_H = (\rho_e v_a \hat{\delta}_H^2/\mu_e R)$ and $X = (x/R)$. In these equations, (1) the changes of the flow with x-direction at the outer edge of the boundary layer; $U = v_{xe}/v_a = f(x/R)$, (2) the dimensionless groups determined from T_w, T_e and ω_{Ae}; (T_w/T_e), $(-\Delta\hat{H}/(\hat{H}_{Aw} - \hat{H}_{Ae}))$, and (3) the Damköhler modulus; $(-M_A R_{Ae} R/\rho_e v_a) = (-M_A A (M_e P \omega_{Ae}/M_A \tilde{R} T_e)^{3/2} R/\rho_e v_a) \exp(-E/\tilde{R}T_e)$ are independent parameters, which should be provided as external factors. The values of U' were calculated from the equation given by Hiementz [20] independently of the temperature condition.

The changes of fluid properties included in the calculations may be expressed as

$$\frac{\mu}{\mu_e} = \left(\frac{\mu_A}{\mu_{Ae}} \right) \left\{ \frac{\omega_A}{\omega_A + (1-\omega_A)\phi_{AB} M_B/M_A} + \left(\frac{\mu_B}{\mu_A} \right) \frac{1-\omega_A}{\omega_A \phi_{BA} M_B/M_A + (1-\omega_A)} \right\} \Bigg/ \left\{ \frac{\omega_{Ae}}{\omega_{Ae} + (1-\omega_{Ae})\phi_{AB} M_B/M_A} + \left(\frac{\mu_{Be}}{\mu_{Ae}} \right) \frac{1-\omega_{Ae}}{\omega_{Ae} \phi_{BA} M_B/M_A + (1-\omega_A)} \right\} \simeq \left(\frac{T}{T_e} \right)^{\beta} \cdot f_v \left\{ \omega_A, \omega_{Ae}, M_A, M_B, \left(\frac{\mu_{Be}}{\mu_{Ae}} \right) \right\}, \tag{34}$$

$$\frac{M}{M_e} = \left\{ \omega_{Ae} \left(\frac{M_B}{M_A} - 1 \right) + 1 \right\} \Big/ \left\{ \omega_A \left(\frac{M_B}{M_A} - 1 \right) + 1 \right\}, \tag{35}$$

and

$$\frac{\rho}{\rho_e} = \left(\frac{M}{M_e}\right)\left(\frac{T_e}{T}\right). \tag{36}$$

By using Ω_M, Ω_D (or ω_{Aw}) and Ω_H calculated by the above mentioned procedure, we get the friction factor and the Nusselt number from equations (19) and (33), respectively. In addition, the Nusselt modulus defined by the enthalpy difference between the wall and the outer edge of the boundary layer is obtained from equation (30), which is related to the usual Nusselt number as

$$\frac{Pr\, q_w R}{(\hat{H}_{Aw}-\hat{H}_{Ae})\mu_e} = \frac{q_w R}{(T_w-T_e)\lambda_e}\frac{\hat{C}_{pe}}{\langle \hat{C}_{pA}\rangle}, \tag{37}$$

where $\langle \hat{C}_{pA}\rangle = (\hat{H}_{Aw}-\hat{H}_{Ae})/(T_w-T_e)$. Thus, as is the case of air or nitrogen, for small changes of $\hat{C}_{pA}$ with temperature difference the modulus is nearly equal to the usual Nusselt number, but in the case of propane the factor $\hat{C}_{pe}/\langle \hat{C}_{pA}\rangle$ changes significantly as the temperature difference increases as shown in Fig. 6. An advantage of the new definition of the Nusselt modulus is shown in the next section.

3.2. *Effect of a large temperature difference*

We will now discuss the effect of a large temperature difference under the assumption of no chemical reaction, that is, $\Delta\hat{H} = 0$, $A = 0$ and $\omega_{Aw} = 1$. The values of the exponents α and β in equations (31) and (34) are taken as $\alpha = 0.095$, $\beta = 0.683$ and $Pr = 0.703$ for nitrogen and $\alpha = 0.593$, $\beta = 0.865$ and $Pr = 0.783$ for propane.

The friction factors are shown in Fig. 7. The variation of the friction factor for propane with the temperature ratio, T_w/T_e, shows a similar trend of that for nitrogen, mainly because the temperature dependencies of the viscosity are similar to each other as seen from Fig. 6. The location of the separation point moves upstream with the increase of the temperature ratio.

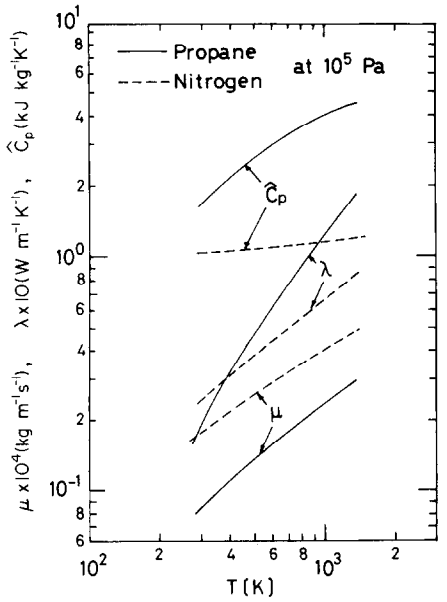

FIG. 6. Changes of viscosities [22], thermal conductivities [23] and specific heat at constant pressure of nitrogen and propane.

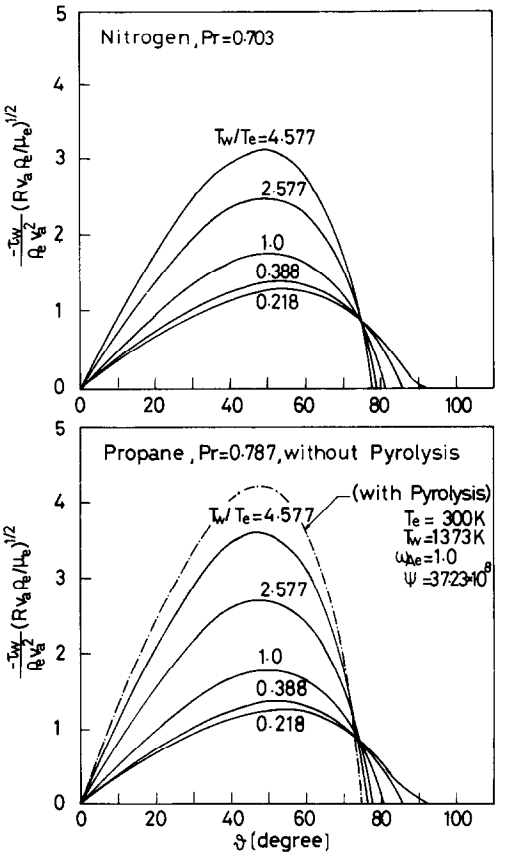

FIG. 7. Circumferential changes of wall shear stress.

Calculated results of the Nusselt number for nitrogen and propane are shown by solid curves in Fig. 8. The variation of the Nusselt number for propane with the temperature ratio is found to be large, whereas that for nitrogen is small, because the temperature dependencies of λ and $\hat{C}_p$ for propane are different from those for nitrogen (Fig. 6).

On the other hand, the Nusselt modulus based on the enthalpy difference shows a small dependence on the temperature ratio for both propane and nitrogen. The calculated results are shown in Fig. 9. As is seen from this figure, the maximum deviations from the value of $T_w/T_e = 1$ is 5% at $T_w/T_e = 4.577$ for propane, and much less for nitrogen.

By using this fact and the relationship of equation (37), we get a simple approximate formula, by which the effect of a large temperature difference on the Nusselt number is calculated, as

$$\frac{Nu}{Nu_0} \simeq \frac{\langle \hat{C}_p\rangle}{\hat{C}_{pe}} \simeq \frac{1}{1+\alpha}\frac{(T_w/T_e)^{1+\alpha}-1}{(T_w/T_e)-1}, \tag{38}$$

where Nu_0 is a Nusselt number at a limiting case of $T_w/T_e = 1$. For the case of propane, the values calculated from equation (38) are depicted at $T_w/T_e = 0.218$ and 4.577 by broken curves in Fig. 8. The conventional correlation based on the fluid properties

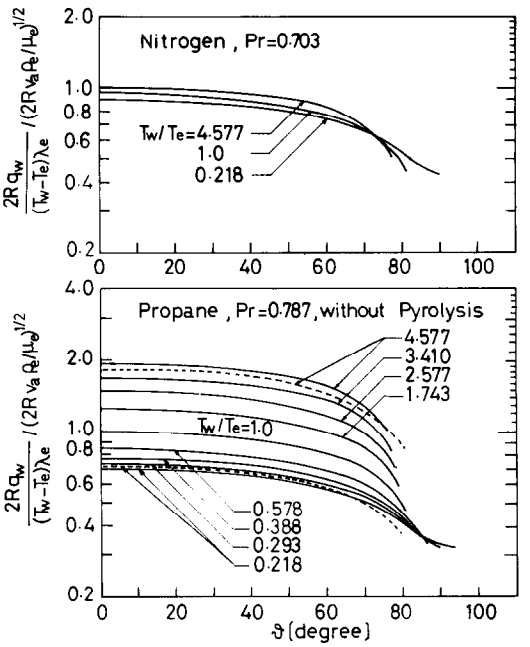

FIG. 8. Circumferential changes of Nusselt number (without pyrolysis).

at film temperature can be expressed by

$$\frac{Nu}{Nu_0} \simeq \left\{\frac{1}{2}\left(1+\frac{T_w}{T_e}\right)\right\}^{\alpha+\beta/2-0.5}. \tag{39}$$

This equation is derived from the relationship of

$$\frac{2Rq_w}{(T_w-T_e)\lambda_f} = \text{const.}\left(\frac{2Rv_a\rho_f}{\mu_f}\right)^{1/2}, \tag{40}$$

and equations (31) and (34), where the subscript f refers to values at the film temperature, $T_f = (T_w+T_e)/2$. The simplest formula of equation (38) seems to be a better approximation of the results of numerical calculations than the correlation using film temperature.

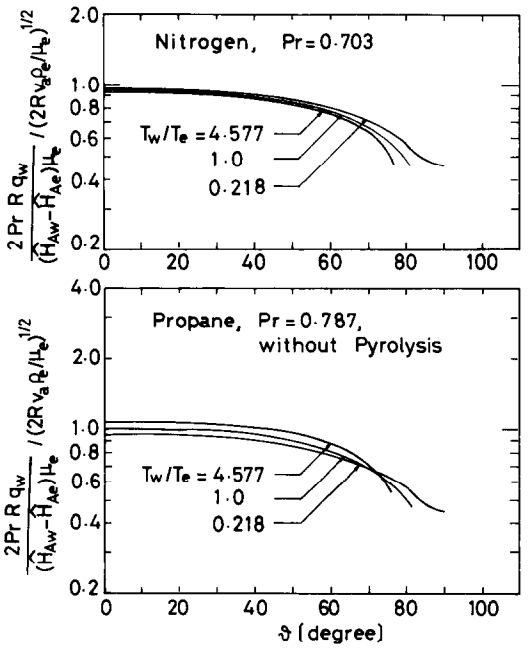

FIG. 9. Circumferential changes of Nusselt modulus based on enthalpy difference (without pyrolysis).

The experimental results of the Nusselt modulus based on the enthalpy difference are compared with the calculated results in Figs. 10(a) and (b) for nitrogen and propane, respectively. The experimental values are the same as the ones presented in Fig. 3. Good agreement between both results are obtained in the case of nitrogen. In the case of propane, the experimental results obtained in the region $2Rv_a\rho_e/\mu_e \leqslant 3\times10^3$ and $T_w/T_e \leqslant 3.41$ ($T_w = 1025$ K) are also in fairly good agreement with the calculated lines. In the region of higher Reynolds numbers, the experimental values are somewhat higher than those of the analytical line, probably because the flow near the edge of the boundary layer becomes turbulent. In the case of $T_w/T_e = 3.910$ and $T_w/T_e = 4.577$, the calculated results, in which the effect of the chemical reaction is ignored, are shown by broken lines. The experimental values are seen to be higher than the calculated ones, showing the effect of pyrolysis.

3.3. *Effect of pyrolysis*

In Fig. 11, the analytical results of the Nusselt modulus are plotted against the Damköhler modulus which shows the effect of chemical reaction. This figure shows that the Nusselt modulus increase with increasing Damköhler modulus; the Nusselt modulus is about 1.3 times as large as that in the chemically inert case when the Damköhler modulus is about 6×10^4 and $T_w = 1373$ K, $T_e = 300$ K.

Comparisons of the analysis and experiments are given in Fig. 10(b). The solid curves of $T_w/T_e = 4.577$ and 3.910 are the analytical results for the present experimental condition of $(-M_A A(p/\hat{R}T_e)^{3/2}R^2/\mu_e) = 5.904\times10^{11}$. The agreement between the calculated and experimental results is fairly good, that is, the effect of pyrolysis on the heat transfer coefficients is well predicted by the present analysis. However, the calculation procedure of the present analysis is too tedious. Therefore, a simplified method for a quick estimation of the effect of pyrolysis is desired. For this purpose, though $\hat{\delta}_H$ changes with the pyrolysis we will make an approximation

$$\left(\frac{\rho_e v_a \hat{\delta}_H^2}{\mu_e R}\right)^{1/2} \simeq \left(\frac{\rho_e v_a \hat{\delta}_H^2}{\mu_e R}\right)^{1/2}_{\substack{\text{without}\\ \text{pyrolysis}}} = 2\sqrt{\left(\frac{Rv_a\rho_e}{\mu_e}\right)\Big/\left(\frac{Pr\, q_w R}{(\hat{H}_{Aw}-\hat{H}_{Ae})\mu_e}\right)_{\substack{\text{without}\\ \text{pyrolysis}}}} \tag{41}$$

From equation (30), we get

$$\left\{\frac{Pr\, q_w R}{(\hat{H}_{Aw}-\hat{H}_{Ae})\mu_e}\Big/\left(\frac{Pr\, q_w R}{(\hat{H}_{Aw}-\hat{H}_{Ae})\mu_e}\right)_{\substack{\text{without}\\ \text{pyrolysis}}} - 1\right\} \times \left(\frac{\hat{H}_{Aw}-\hat{H}_{Ae}}{-\Delta\hat{H}}\right)\frac{Sc_e}{Pr} = \frac{\omega_{Ae}K_{AB}+1}{K_{AB}} \ln\left(\frac{\omega_{Ae}K_{AB}+1}{\omega_{Aw}K_{AB}+1}\right). \tag{42}$$

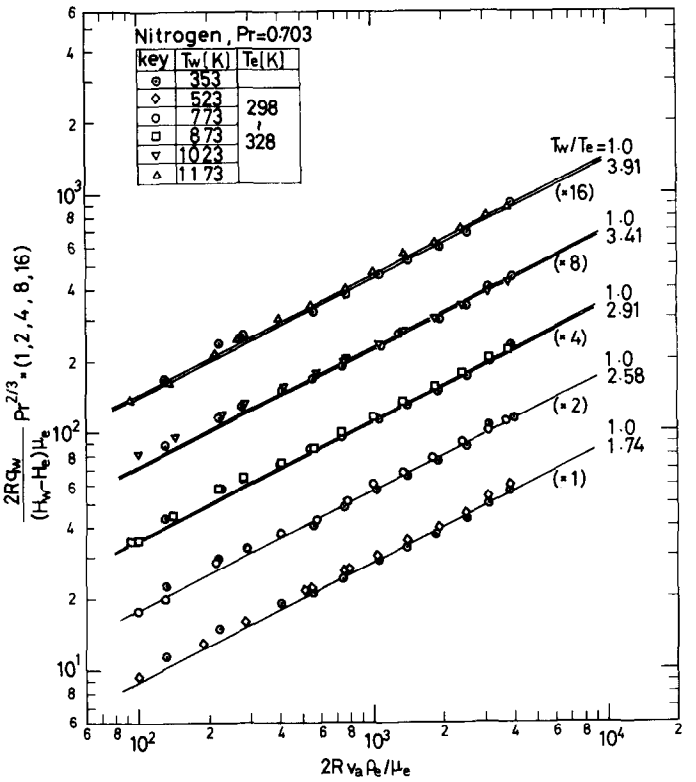

FIG. 10(a). Correlations of experimental and calculated results of Nusselt modulus based on enthalpy difference at $\theta = 55°$.

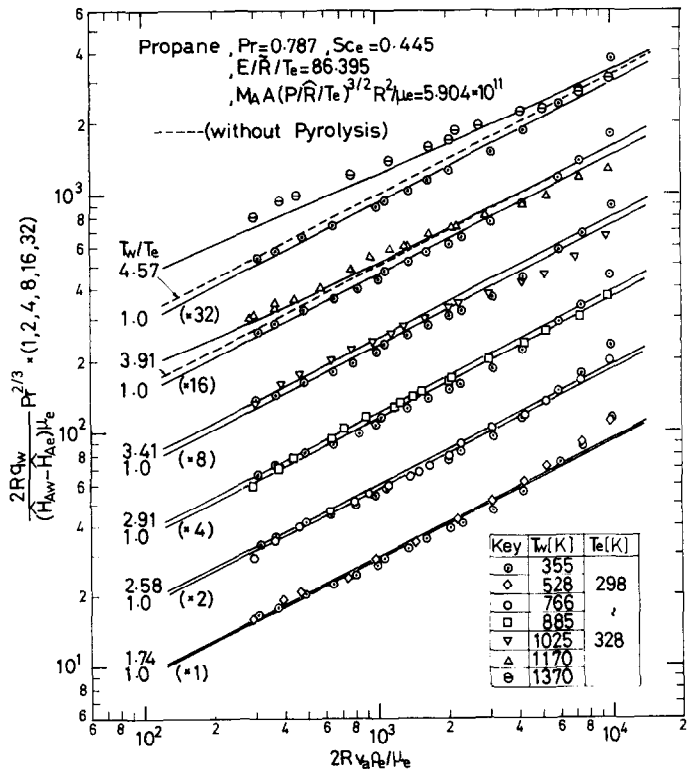

FIG. 10(b). Correlations of experimental and calculated results of Nusselt modulus based on enthalpy difference at $\theta = 55°$.

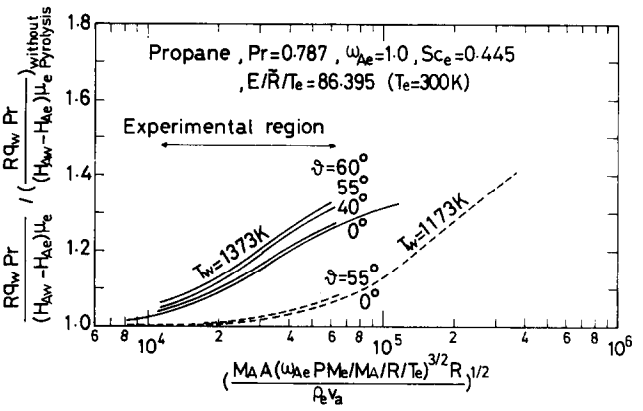

FIG. 11. Changes of Nusselt modulus with Damköhler modulus.

On the other hand, by assuming $R_{Aw} \gg R_{Ae}$ and using equations (21) and (34), equation (25) may change

$$\left(-M_A A\left(\omega_{Ae}\frac{M_e}{M_A}\frac{P}{\hat{R}T_e}\right)^{3/2}R^2/\mu_e\right)\exp\left(-\frac{E}{\tilde{R}T_w}\right)\times\left(\frac{T_w}{T_e}\right)^{\beta-3/2}Sc_e\,\Omega_D\left(\frac{\mu_e}{Rv_a\rho_e}\right)$$
$$= 12\frac{\omega_{Ae}K_{AB}+1}{K_{AB}}\times\ln\left(\frac{\omega_{Ae}K_{AB}+1}{\omega_{Aw}K_{AB}+1}\right)\Big/\left(\frac{M_w}{M_e}\frac{\omega_{Aw}}{\omega_{Ae}}\right)^{3/2}f_v. \quad (43)$$

Using equation (41) with a further approximation of $\hat{\delta}_D \simeq \hat{\delta}_H$ and eliminating ω_{Aw} from equations (42) and (43), we obtain a general relationship between

$$\left\{\frac{Pr\,q_wR}{(\hat{H}_{Aw}-\hat{H}_{Ae})\mu_e}\Big/\left(\frac{Pr\,q_wR}{(\hat{H}_{Aw}-\hat{H}_{Ae})\mu_e}\right)_{\substack{\text{without}\\\text{pyrolysis}}}-1\right\}\times\left(\frac{\hat{H}_{Aw}-\hat{H}_{Ae}}{-\Delta\hat{H}}\right)\frac{Sc_e}{Pr}$$

and

$$4\left\{\frac{-M_AA((M_e/M_A)\omega_{Ae}(P/\hat{R}T_e))^{3/2}R^2}{\rho_eD_{AB_e}}\right\}\times\exp\left(-\frac{E}{\tilde{R}T_w}\right)\left(\frac{T_w}{T_e}\right)^{\beta-3/2}\Big/\left(\frac{Pr\,q_wR}{(\hat{H}_{Aw}-\hat{H}_{Ae})\mu_e}\right)_{\substack{\text{without}\\\text{pyrolysis}}}.$$

The relationship is depicted in Fig. 12 by the dot-dashed curve. Solid and broken curves are the calculated results by the foregoing boundary-layer analysis. The present simplified theory assuming $\hat{\delta}_H = \hat{\delta}_D = \text{const.}$ independently of pyrolysis leads to somewhat larger changes of the Nusselt modulus, but effects of all parameters are expressed in one curve.

4. CONCLUSION

Several results of experimental and analytical investigations concerning heat transfer between a cylinder and transverse flows of nitrogen and propane have been presented. To conclude the investigations, we may summarize the results as follows:

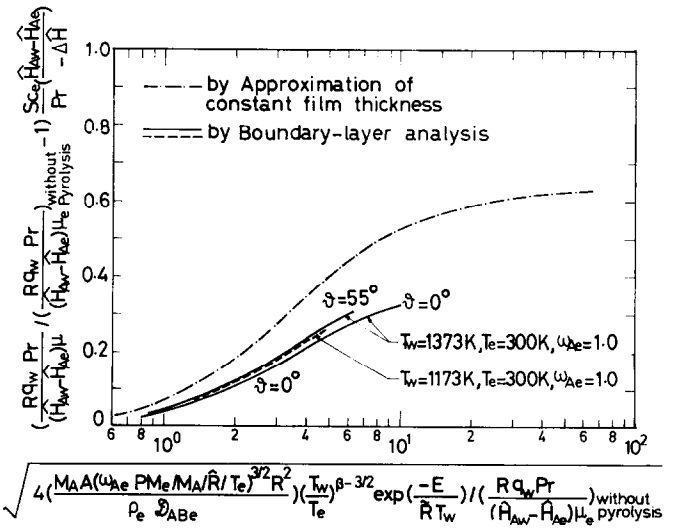

FIG. 12. Comparison between calculated results by boundary-layer analysis and by simplified method for changes of Nusselt modulus with pyrolysis.

(1) In the flow of nitrogen, the effect of the temperature difference on the Nusselt number is small.

(2) In the flow of propane, the Nusselt number changes significantly with increasing wall temperature, though the temperature is within the range of the chemically inert temperature. At a higher wall temperature, pyrolysis of propane near the wall causes an appreciable heat transfer increase at a small Reynolds number.

(3) For the effect of a large temperature difference on Nusselt number, simpler formula than a conventional film-temperature correlation was obtained as shown in equation (38). Furthermore, it is recommended that the Nusselt modulus defined by the enthalpy difference is used because it does not change with wall temperatures in both inorganic and organic gas flows.

(4) For the effect of pyrolysis, the experimental results are well represented by the analysis using a simple model for the reactions and gas compositions. A simpler analysis similar to the film theory assuming a constant film thickness results in the over-estimate of the heat transfer coefficient, but may be useful for a simplified prediction.

Further experimental investigations at an elevated ambient temperature are desired for industrial applications.

REFERENCES

1. E. Schmidt and K. Wenner, Wärmeabdabe üoer den Umfang eines angeblasenen geheizten Zylinders, *ForshArb. GebIngWes.* **12,** 65–73 (1941).
2. E. R. G. Eckert and E. Soehngen, Distribution of heat transfer coefficients around circular cylinder in crossflow at Reynolds number from 20 to 500, *Trans. Am. Soc. Mech. Engrs* **74,** 343–347 (1952).
3. K. M. Krall and E. R. G. Eckert, Local heat transfer around a cylinder at low Reynolds number, *Trans. Am. Soc. Mech. Engrs*, Series C, *J. Heat Transfer* **95,** 273–275 (1973).
4. N. Frössling, Verdunstung Wärmeübergang und Geschwindigkeitsverteilung bei zweidimensionaler und rotationssymmetricher laminarer Grenzschitstromung, *Lunds Univ. Arsskr., Avd 2* [*N.F.*] **36,** 1 (1940).
5. Von W. Dieneman, Brechnung des Wärmeüberganges an laminar umstromten Körpern mit konstanter und ortsveränderlicher Wandtemperature, *Z. Angew. Math. Mech.* **33,** 89–109 (1953).
6. S. W. Churchill and J. C. Brier, Convective heat transfer from a gas stream at high temperature to a circular cylinder normal to the flow, *Chem. Engng Prog. Symp. Ser.* **51,** 57–66 (1955).
7. W. J. M. Douglas and S. W. Churchill, Recorrelation of data for convective heat transfer between gases and single cylinders with large temperature difference, *Chem. Engng Prog. Symp. Ser.* **52,** 23–28 (1956).
8. R. I. Rothenberg and J. M. Smith, Dissociation and heat transfer in laminar flow, *Can. J. Chem. Engng* **44,** 67–73 (1966).
9. W. Schotte, Heat transfer to a gas-phase chemical reaction, *Ind. Engng Chem.* **50,** 683–690 (1958).
10. P. L. T. Brian and R. C. Reid, Heat transfer with simultaneous chemical reaction: film theory for a finite reaction rate, *A.I.Ch.E. Jl* **8,** 322–329 (1962).
11. P. L. T. Brian, Turbulent pipe flow heat transfer with a simultaneous reaction of finite rate, *A.I.Ch.E. Jl* **9,** 831–842 (1963).
12. Y. Tambour, Transport coupling theory for multicomponent non-equilibrium chemically reacting boundary layers, *Physics Fluids* **22,** 1255–1260 (1979).
13. J. A. Fay and F. R. Ridell, Theory of stagnation point heat transfer in dissociated air, *J. Aeronaut. Sci.* **25,** 73–85 (1958).
14. L. Lees, Laminar heat transfer over blunt-nozed bodies at hypersonic flight speed, *Jet Propul.* **26,** 259–269 (1956).
15. P. L. T. Brian, R. C. Reid and S. W. Bodman, Heat transfer to decomposing nitrogen oxide in a turbulent boundary layer, *A.I.Ch.E. Jl* **11,** 809–814 (1965).
16. G. R. Bopp and D. B. Mason, Experimental natural convection heat transfer from wire to the nonequilibrium chemically reacting system: NO_2–NO–O_2, *Ind. Engng Chem. Fundam.* **4,** 222–224 (1965).
17. L. L. Edwards and R. R. Furgason, Heat transfer in thermally decomposing ozone, *Ind. Engng Chem. Fundam.* **7,** 440–445 (1968).
18. T. Mizushina, T. Matsumoto, Y. Ono and K. Kamei, Experimental study of spray quenching: Cooling experiment of pyrolysis gas of propane, *Asahi Garasu Kogyo Gihitsu Shorei-Kai Kenkyu Hokoku* **31,** 19–31 (1977).
19. J. Fujita, Comparison of equations for diffusion coefficients in gaseous systems, *Kagaku Kogaku* **28,** 251–254 (1964).
20. K. Hiementz, *Modern Developments in Fluid Dynamics* (edited by S. Goldstein), Vol. 1, p. 150. Clarendon Press, Oxford (1950).
21. L. A. Bromley and C. R. Wilke, Viscosity behaviour of gases, *Ind. Engng Chem.* **43,** 1641–1648 (1951).
22. L. I. Steil and G. Thodos, The viscosity of nonpolar gases at normal pressure, *A.I.Ch.E. Jl* **7,** 611–615 (1961).
23. D. Misic and G. Thodos, The thermal conductivity of hydrocarbon at normal pressure, *A.I.Ch.E. Jl* **7,** 264–267 (1961).

EFFET D'UNE GRANDE DIFFERENCE DE TEMPERATURE ET DE LA PYROLYSE SUR LE TRANSFERT THERMIQUE ENTRE UN CYLINDRE ET UN ECOULEMENT TRANSVERSAL DE GAZ D'AZOTE ET DE PROPANE

Résumé—L'étude expérimentale et analytique a été faite pour la région frontale de la couche limite sur un cylindre chauffé, normal à l'écoulement d'un gaz. Dans les écoulements de gaz propane, le nombre de Nusselt usuel croît significativement avec l'augmentation de la température pariétale, au contraire des petites variations dans le cas de l'azote. Ceci est dû à la différence des dépendances des propriétés du fluide entre les deux gaz et à la pyrolyse du propane aux températures de paroi élevées, aux grands modules de Damköler. Les résultats sont bien représentés par l'analyse de la couche limite utilisant des modèles simples pour les réactions et les compositions du gaz. On montre que les mesures pour l'azote et le propane aux faibles modules de Damköler sont bien représentés, indépendamment des conditions de température, en utilisant le module de Nusselt défini par une différence d'enthalpie. Les expériences avec un cylindre chauffé de 5 mm de diamètre et avec les écoulements à la température de la salle et à la pression atmosphérique, correspondent à des nombres de Reynolds entre 10^2 et 10^4 et à des rapports de température T_w/T_e entre 1,743 et 4,577.

DER EINFLUSS EINER GROSSEN TEMPERATURDIFFERENZ UND THERMISCHER ZERSETZUNG AUF DEN WÄRMEÜBERGANG AN EINEM QUER VON STICKSTOFF UND PROPANGAS ANGESTRÖMTEN ZYLINDER

Zusammenfassung—Für der vorderen Grenzschichtbereich eines beheizten, quer zum kalten Gasstrom angeordneten Zylinders wurden experimentelle und analytische Untersuchungen angestellt. Bei der Propangasströmung steigt die Nusselt-Zahl stark mit steigender Wandtemperatur im Gegensatz zu nur schwachen Veränderungen bei der Stickstoffströmung. Dies ist auf die unterschiedliche Temperaturabhängigkeit der Stoffwerte beider Gase und auf die thermische Zersetzung des Propans bei höheren Wandtemperaturen zurückzuführen, vornehmlich bei großen Damköhler-Zahlen. Die Ergebnisse lassen sich durch eine Grenzschichtbetrachtung mit einfachen Modellen für Reaktion und Gaszusammensetzung gut wiedergeben. Es wird gezeigt, daß die Ergebnisse für Stickstoff und Propangas bei kleinen Damköhler-Zahlen durch eine mit der Enthalpiedifferenz gebildete Nusselt-Zahl temperaturunabhängig korreliert werden können. Die Versuche mit einem Zylinder von 5 mm Durchmesser und Strömungen von Raumtemperatur und Umgebungsdruck lagen in einem Bereich der Reynolds-Zahl von 10^2 bis 10^4 und bei Temperaturverhältnissen T_w/T_e von 1,743 bis 4,577.

ВЛИЯНИЕ БОЛЬШОЙ РАЗНОСТИ ТЕМПЕРАТУР И ПИРОЛИЗА НА ТЕПЛОПЕРЕНОС МЕЖДУ ЦИЛИНДРОМ И ПОПЕРЕЧНЫМИ ПОТОКАМИ АЗОТА И ПРОПАНА В ГАЗООБРАЗНОМ СОСТОЯНИИ

Аннотация—Проведены экспериментальные и аналитические исследования передней области пограничного слоя вокруг нагретого цилиндра при поперечном обтекании холодным потоком газа. При обтекании цилиндра газообразным пропаном значения числа Нуссельта существенно возрастали с ростом температуры стенки по сравнению с их очень незначительным увеличением при обтекании азотом. Это объясняется различной зависимостью свойств обоих газов от температуры, а также пиролизом пропана при высоких температурах стенки, т.е. при больших значениях числа Дамкёлера. Полученные результаты хорошо описываются теорией пограничного слоя с помощью простых моделей реакций и состава газов. Также показано, что независимо от температуры данные как для азота, так и пропана при малых значениях числа Дамкёлера хорошо описываются числом Нуссельта, выраженным через разность энтальпий. Эксперименты, в которых использовался нагретый цилиндр диаметром 5 мм, обтекаемый потоками газов при комнатной температуре и атмосферном давлении, проводились в диапазонах числа Рейнольдса от 10^2 до 10^4 и отношения температур T_w/T_e от 1,743 до 4,577.